Lysine-derived Charge-Altering Releasable Transporters (K-CARTs): Targeted Delivery of mRNA and siRNA to the Lungs

Timothy R. Blake ^{1a}, Ole A. W. Haabeth ^{1b}, Adrienne Sallets ^b, Rebecca L. McClellan ^a, Trevor J. Del Castillo ^a, Jose G. Vilches-Moure ^d, Wilson C. Ho ^a, Paul A. Wender ^{a,c}, Ronald Levy ^b, Robert M. Waymouth* ^{a, 2}

aDepartment of Chemistry, Stanford University, Stanford, CA 94305;
bDivision of Oncology, Department of Medicine, Stanford Cancer Institute, Stanford University, Stanford, CA 94305;
and cDepartment of Chemical and Systems Biology, Stanford University, Stanford, CA;
and dDepartment of Comparative Medicine, Stanford University, Stanford, CA 94305
Email: waymouth@stanford.edu

Abstract

Targeted delivery of nucleic acid therapeutics to the lungs could transform treatment options for pulmonary disease. We have previously developed oligomeric charge-altering releasable transporters (CARTs) for in vivo mRNA transfection and demonstrated their efficacy for use in mRNA-based cancer vaccination and local immunomodulatory therapies against murine tumors. While our previously reported glycine-based CART-mRNA complexes (G-CARTs/mRNA) show selective protein expression in the spleen (mouse, >99%), here we report a new lysine-derived CART-mRNA complex (K-CART/mRNA) that, without additives or targeting ligands, shows selective protein expression in the lungs (mouse, >90%) following systemic IV administration. We further show that by delivering siRNA using the K-CART we can significantly decrease expression of a lung-localized reporter protein. Blood chemistry and organ pathology studies demonstrate that K-CARTs are safe and well-tolerated. We report on the new step economical, organocatalytic synthesis (two steps) of functionalized polyesters and oligocarbonate-co-α-aminoester K-CARTs from simple amino acid and lipid-based monomers. The ability to direct protein expression selectively in the spleen or lungs by simple, modular changes to the CART structure opens fundamentally new opportunities in research and gene therapy.

Keywords: organ targeting, carriers, nonviral vectors, cellular selectivity, gene therapy

Introduction

Nucleic acid therapies are increasingly being evaluated in promising new approaches to the prevention and treatment of infectious disease¹⁻⁶ as highlighted by the rapid clinical translation of mRNA vaccines to curb the SARS-CoV-2 pandemic.⁷ Of further significance, nucleic acid therapies present potentially transformative approaches for the treatment of autoimmune⁸ and genetic disease⁹ as well as cancer.¹⁰⁻¹⁴ However, a key to the further implementation of this technology will require selective delivery to and functional expression of oligonucleotides such as mRNA in specific organs and cell populations of interest.¹⁵⁻¹⁸ For example, functional expression of nucleic acid therapeutics in the lungs would provide interventions for pulmonary disease, including lung cancer, asthma,¹⁹ and cystic fibrosis.²⁰ Thus, achieving targeted delivery and functional expression of nucleic acids in specific organs, such as the lung, is a formidable barrier to realizing the full potential of mRNA therapeutics.^{8, 11, 14-15, 21}

While local administration²²⁻²⁴ and the attachment of targeting ligands²⁵⁻²⁹ are being actively pursued, there is growing evidence that manipulation of the inherent physico-chemical properties of the delivery vehicle itself can influence both the organs and cell types that are transfected upon systemic administration.^{15-16,30-37} For example, we have previously reported on a family of diblock copolymers called charge-altering releasable transporters (CARTs)^{10, 22, 38-45} that are effective delivery vehicles for mRNA, circRNA,⁴² pDNA,⁴⁰ and multiple polyanionic cargos.²² We have demonstrated that tuning the structural identity of the lipid block or initiator of the CART impacts the transfection efficiency of the CART for different cell types.⁴⁴⁻⁴⁵ N-hydroxyethyl glycine-derived CARTs (previously described³⁸ but newly referred to here as **G-CARTs**, vide infra) and serine-derived CARTs³⁹ elicit protein expression in the spleen with high selectivity (>99%) upon intravenous (IV) tail vein injection in mice, providing an example of extrahepatic mRNA delivery by a non-viral vector. We also demonstrated the utility of these **G-CARTs** as therapeutic agents by curing antigen-expressing murine tumors (OVA⁺-A20) with mRNA-based cancer vaccination,¹⁰ in novel local mRNA-based immunomodulatory cancer therapies as a model for metastatic disease,²² and by developing a prophylactic mRNA vaccine for SARS-CoV-2.⁴³

Herein we describe a new class of CARTs (**K-CARTs**) that, upon complexation with mRNA and systemic delivery (mice), provide selective protein expression in the lungs. In addition to this profound change in organ selectivity (from >99% spleen to >90% lung) as a function of only changes in the CART components, the chemical modification from a glycine-based α -amino

ester repeat unit (thus **G-CART**, **Figure 1a**) to a <u>lysine</u>-based α -amino ester repeat unit (thus **K-CART**, **Figure 1b**) has been found to influence the rate and mechanism of degradation of the amphiphilic CART oligomer as well as the size, zeta potential and dynamics of the resulting complexes with mRNA. Understanding the interplay of these physicochemical properties and the resulting biological activity of nucleic acid delivery vectors is critical for the further development of gene therapies. Additionally, inspired by the clinical success of siRNA-based therapies⁴⁶ and indicative of the generality of CARTs as a platform technology for gene (polyanion) delivery, we demonstrate the functional in vivo delivery of siRNA to the lung with **K-CART**/siRNA nanoparticles.

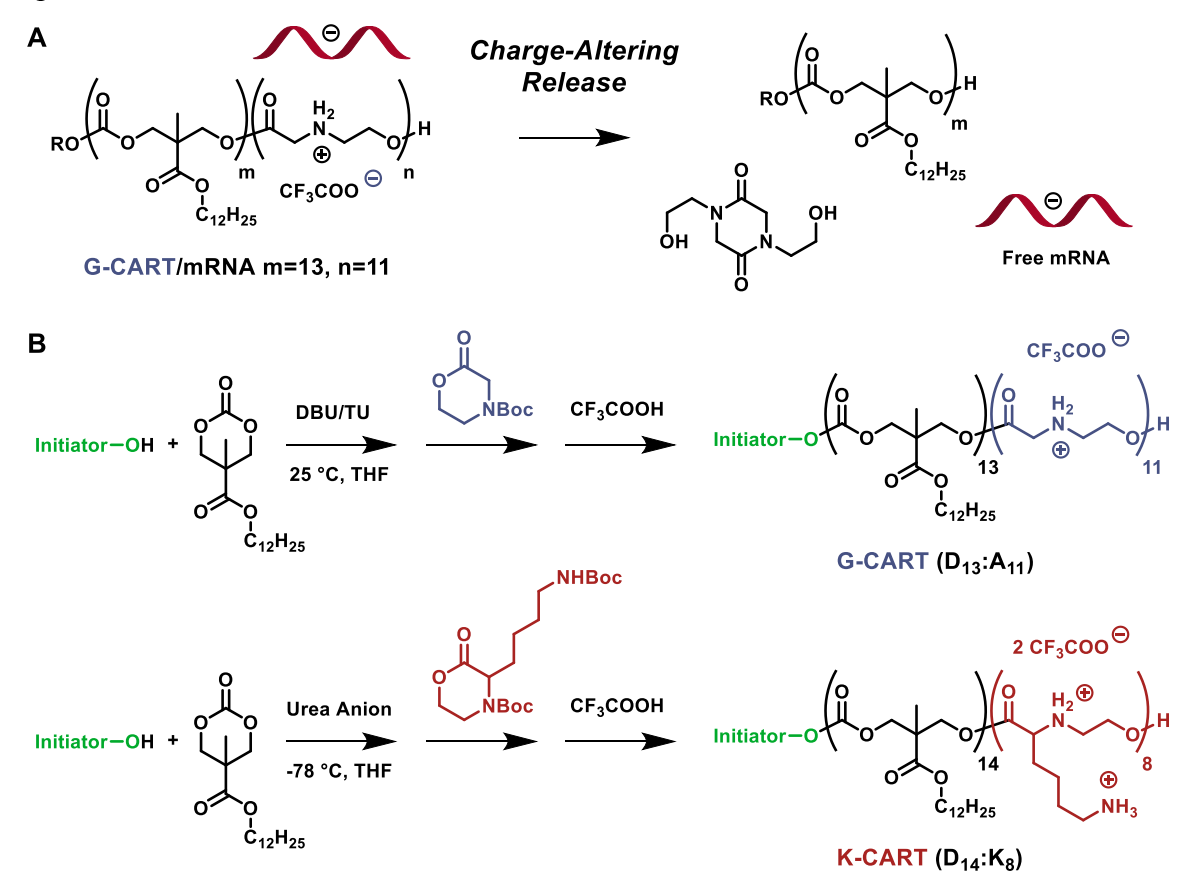


Figure 1. CART/mRNA delivery concept and synthesis of new CARTs. A.) Amphiphilic CART oligomers complexed to mRNA at pH 5.5 release mRNA under physiological conditions (pH 7.4) by charge-altering degradation of the hydroxyethyl glycine repeat unit. B.) Organo-catalytic ring-opening polymerization (OROP) and deprotection strategy for the syntheses of **G-CART** (D_{13} : A_{11}) and novel **K-CART** (D_{14} : K_8).

Results

We modified a previously developed synthetic route⁴¹ to generate lysine-derived morpholinone monomers and their co-polymerization with lipid-functionalize cyclic carbonates to generate CART amphiphiles derived from lysine. As previous studies had revealed that the nature of lipid sequences of the CART amphiphiles influenced the cell selectivity of mRNA expression,⁴⁴ these studies were initiated to assess if the charge density and the nature, number and spatial array of the cationic repeat units would influence delivery to and transfection and mRNA translation in different cell types and organs.

Prior to generating the amphiphilic lysine CARTs (**Figure 1B**), we first investigated the synthesis and properties of the poly(N-hydroxyethyl-lysine) **p(heK)**²⁺ homopolymer **5** prepared from the lysine-derived morpholinones (**Figure 2B**). In these studies, we compared the synthesis and degradation of the previously reported⁴¹ poly(N-hydroxyethyl-glycine) **p(heG)**⁺ **6** to that of poly(N-hydroxyethyl-lysine) **5** (**Figure 2C**). The morpholinone monomers were prepared by a three-step sequence from 2-bromoethanol and the desired amino acid methyl ester, as its HCl salt (**Figure 2A**). Morpholinone **3a** (R = H, derived from N-hydroxyethyl glycine) was previously prepared by the oxidative lactonization of N-substituted diethanolamines;³⁸ the present synthesis provides a more general route to amino acid-derived morpholinones.⁴¹ This three-step procedure afforded the glycine-derived morpholinone **3a** in an overall yield of 34% and the lysine-derived morpholinone **3b** in 47% overall yield.

Attempts to polymerize the morpholinone **3b** under conditions reported for morpholinone **3a** $^{10, 38, 47}$ were unsuccessful (R.T. with thiourea / DBU organocatalysts). We reasoned that this was due to unfavorable polymerization thermodynamics of the substituted morpholinones. $^{41, 47-48}$ Based on the hypothesis that the unfavorable entropy of polymerization of **3b** at ambient temperature was limiting conversion of this monomer, $^{48-50}$ we employed more reactive organic catalysts 51 derived from urea anions and carried out the polymerization at -78°C (**Figure 2B**). Polymerization of **3b** with a benzyl alcohol initiator and a phenyl cyclohexyl urea anion catalyst in THF cooled by a dry ice/acetone bath ([**3b**] $_0$ = 1 M, [urea] $_0$ = 0.08 M, [KH] $_0$ = 0.0266 M [BnOH] = 0.01 M) proceeded over 20 minutes to convert ca. 60% of **3b** and generate the N-hydroxylethyl lysine homopolyester **4** in ca. 50% total isolated yield, after dialysis. Analysis of the resulting polymer by 1 H NMR and gel permeation chromatography yielded an average degree of polymerization DP = 43.5 with a number average molecular weight (vs. polystyrene) Mn (GPC) =

5.5 kDa and a dispersity $\Theta = 1.2$. The N-Boc-protected polymer 4 was deprotected with 10% TFA in DCM for 4 hours to afford only the cationic homopolymer 5 as a white foam. Analysis by ¹H NMR spectroscopy revealed the quantitative removal of the N-Boc protecting group, but no loss in the average degree of polymerization (DP = 42).

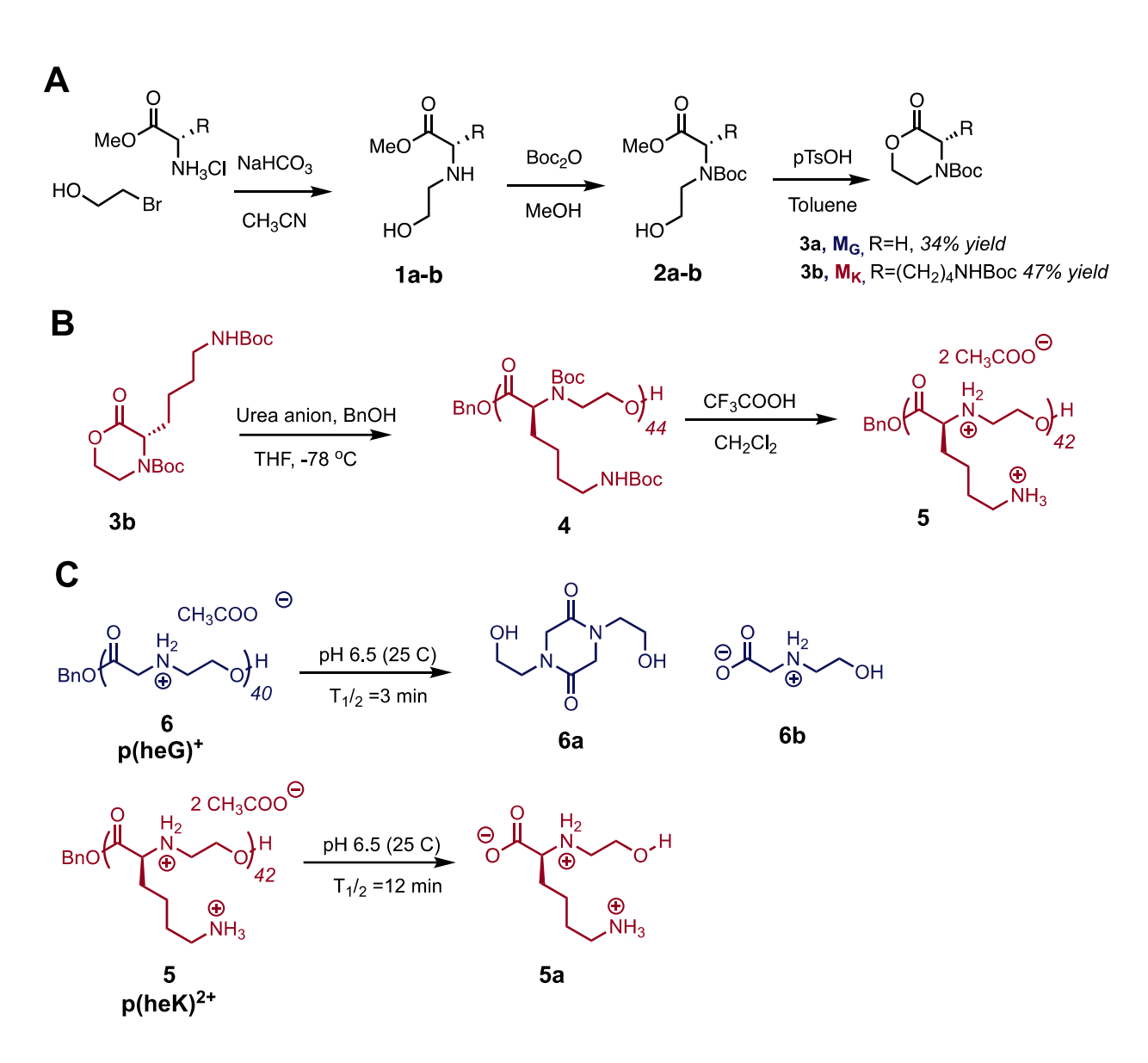


Figure 2. Amino acid-based synthesis of functionalized morpholinone monomers and homopolymers. A) Synthetic pathway for amino acid-sourced monomer synthesis. B) Polymerization and deprotection of cationic homopolymer **5** C) Comparative kinetics and product distributions for the aqueous (pH 6.5) degradation of **6** and **5**.

The cationic homopolymer **5** is readily soluble and stable for >18 h when dissolved in unbuffered D_2O as determined by NMR, and shows similar stability and resistance to hydrolysis to **6** reported previously (stable in D_2O >48 hrs.). However, in phosphate buffered D_2O at pH 6.5 ((K_2HPO_4/KH_2PO_4) = 3.3 M), the lysine-derived **5** degrades selectively (>99 % yield) with first-order kinetics to afford the N-hydroxyethyl lysine zwitterion with a half-life of $t_{1/2}$ =12 min (**Figure 2C**). Illustrative of the intrinsic structural control over release rates, this behavior contrasts that of the related N-hydroxyethyl glycine homopolymer **6**, 38, 41 which degrades more rapidly (pH 6.5, $t_{1/2}$ =3 min) to the diketopiperazine (85% selectivity) along with minor amounts of the N-hydroxyethyl glycine. (**Figure S1**).

Synthesis and characterization of lysine-derived K-CART (D₁₄:K₈) and CART/mRNA nanoparticles. The amphiphilic K-CART (D₁₄:K₈: Figure 1b) was prepared by the low-temperature (-78°C) organocatalytic co-oligomerization of MTC-dodecyl and N-Boc protected morpholinone M_K. The resulting N-Boc-protected oligomer was purified by dialysis, and deprotected with trifluoroacetic acid to afford (>99% yield) the amphiphilic, diblock copolymer K-CART D₁₄:K₈ (Figure 1B) comprised of lipid and dicationic repeat units. The deprotected material was dissolved in DMSO and mixed with mRNA at an overall +/- charge ratio of 10:1 in PBS pH 5.5 to form K-CART/mRNA nanoparticles (NPs) (Figure 3A). The physical properties of the K-CART/mRNA NPs were then compared with that of the previously reported G-CART/mRNA NPs.

As has been previously observed for **G-CART**/mRNA NPs,⁴⁴ characterization of the **K-CART**/mRNA NPs reveals complete complexation of RNA when formulated at this charge ratio (>99% by Qubit RNA assay, **Figure S2**). The size and surface charge of **CART**/mRNA complexes were characterized by dynamic light scattering (DLS) and zeta potential measurements. To assess how size and surface charge evolve over time, we allowed the **CART**/mRNA NPs to stand in pH 7.4 serum-free media or ultrapure D.I. water and monitored changes in the size and zeta potential, respectively, for the two **CART**/mRNA NPs. When **CART**/mRNA NP complexes were analyzed by DLS, **G-CART** NPs showed a mean diameter of 227 (+/- 5) nm, which grew to 470 nm over 2.5 hours, while **K-CART** NPs were slightly smaller at 170 (+/- 3) nm and grew only modestly to 210 nm over 2.5 hours (**Figure 3B, Figure S3**). As previously reported,³⁸ **G-CART** NPs initially exhibit a positive zeta potential of ca. +30 (+/- 2) mV which is neutralized after 20 minutes and

decreases to ca. -30 (+/- 8) mV after two hours (**Figure 3C**). The **K-CART** NPs exhibit a similar initial surface charge of +35 (+/- 3) mV yet retain their positive charge over the two-hour experiment (+30 (+/- 14) mV at two hours). These data helped validate our hypothesis that the more densely cationic **K-CART** results in an altered size, charge, and stability profile of the NPs generated upon mixing with mRNA.

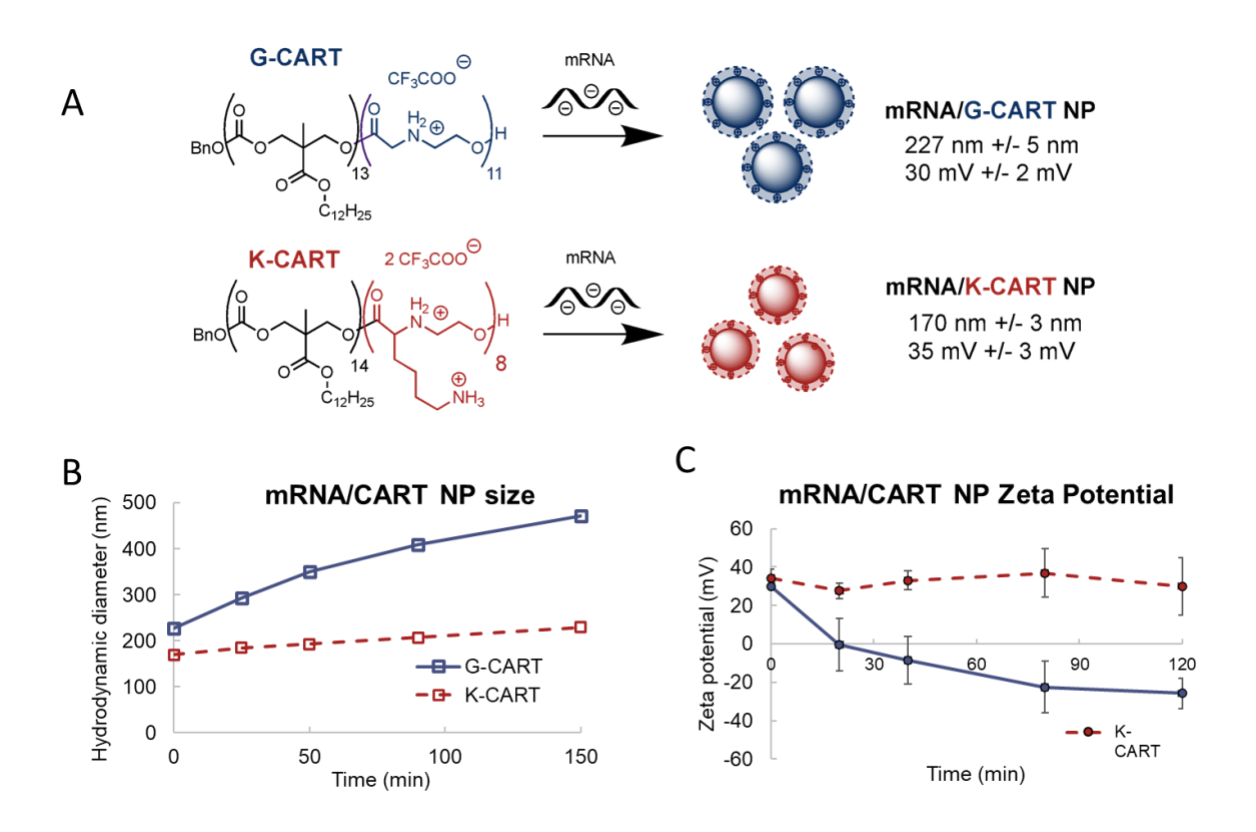


Figure 3. *CART/mRNA NP formulation and stability* studies. A.) CART formulation of NPs via simple mixing of mRNA and CARTs in a 10:1 +/- charge ratio B.) DLS sizing comparison over time between the **G-CART** and **K-CART/mRNA** NPs, open symbols are used to indicate uncertainty, standard deviations are smaller than the symbol size C.) Zeta potential measurements over time for **G-CART** and **K-CART/mRNA** NPs. All measurements are an average of three independent formulations, error bars represent standard deviation.

In vitro K-CART mediated delivery of mRNA. To evaluate the effectiveness of the new K-CART (D₁₄:K₈) as an mRNA delivery vehicle in cell culture and to compare its effectiveness relative to that of G-CART (D₁₃:A₁₁), the CARTs were mixed with mRNA encoding firefly luciferase (FLuc; K-CART/FLuc and G-CART/FLuc) at an overall +/- charge ratio of 10:1 in PBS pH 5.5 then administered to dendritic (DC 2.4), HeLa, or Lewis lung carcinoma (LLC) cells

and assayed for protein expression via bioluminescence imaging (BLI). These studies showed the significant influence of CART structure on reporter gene expression in different cell types: Fluc expression in LLC cells was higher with the **K-CART** than with the **G-CART**, whereas in HeLa cells and DC 2.4 dendritic cells, Fluc expression was higher with the **G-CART** (**Figure S4A**). Importantly, using an MTT cellular proliferation assay, CART/FLuc NPs, the CART vehicles alone, and the degradation product hydroxyethyl lysine show no significant cell toxicity at the doses administered for in vitro studies (1 ng mRNA/1000 cells, **Figure S4B**).

K-CART/FLuc and G-CART/FLuc exhibit strikingly different organ-level protein **expression for mRNA delivery in vivo.** We have previously shown that, upon intravenous injection into the tail-vein (IV) of mice, the G-CART/FLuc exhibits very high selectivity (99%) for protein expression in the spleen. To evaluate the in vivo mRNA delivery with K-CART and to compare it with that of G-CART, we systemically administered K-CART/FLuc in mice by tail vein injection (Figure 4A). After 8 hours, protein expression, as determined by BLI, gave a higher overall signal with G-CART/FLuc (Figure 4B). However, and significantly, the K-CART/FLuc showed a striking predominance of luciferase reporter signal in the lung. After taking full body measurements, mice were sacrificed, and the heart, kidney, liver, lungs, and spleen were harvested to assay the relative luminescence of individual organs (Figure 4C). Remarkably, while protein expression with the G-CART/FLuc localized in the spleen (>99%), in this comparative study the K-CART/FLuc-treated mice predominantly produced reporter signal in the lungs (ca. 91%) with low levels of expression in the spleen (ca. 8%) (Figure 4D) and near-background levels in the liver (ca. 1%). Importantly, no abnormalities were noted upon histo-pathological assessment of tissues and blood taken from mice 72 hours after treatment with K-CART/mRNA (SEAP mRNA, Figure S5).

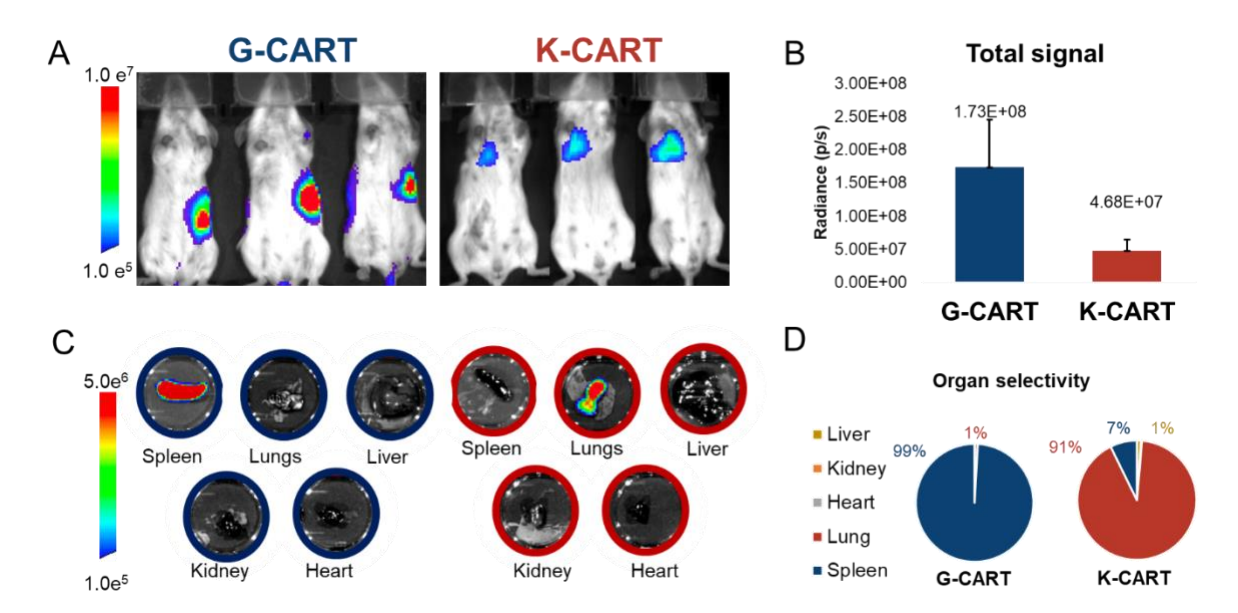


Figure 4. Protein expression induced by **G-CART/FLuc** and **K-CART/FLuc** upon IV injection administration. A.) Representative bioluminescence images (units in radiance) of mice 8 hours after IV injection with 5 ug FLuc mRNA (0.25 mg/kg) formulated with **G-CART** and **K-CART** at an overall +/- charge ratio of 10:1. B.) Overall BLI signal from FLuc/CART-treated mouse immediately before sacrifice (n=3). C.) Representative organ BLI of mice sacrificed 8 hours after mRNA delivery with **G-CART** (left) vs **K-CART** (right) (n=1, see also **Figure S6**) D.) Percent distribution of BLI signal from the organs (n=3) as shown in panel C. (The percent organ distribution was determined by dividing the BLI signal for heart, kidney, liver, lungs, spleen by the total signal of these organs combined).

To perform a more detailed analysis of the cell-level biodistribution of **K-CART**/FLuc in the lung and spleen, we synthesized a benzodiketonate (BDK) fluorophore-functionalized BDK-**K-CART**. The high quantum yield-BDK fluorophore was incorporated into the **K-CART** by use as a BDK-derived initiator, providing covalent attachment to each CART oligomer (**Figure S7**).⁵² In line with the organ-localized BLI measurements, this experiment revealed that ~25% of all the cells in the lungs and ~ 5% of spleen cells were BDK-positive after treatment with BDK-**K-CART**/mRNA whereas > 15% of all cells in the spleen and ~2 % of all lung cells were BDK positive after treatment with BDK-**G-CART**/mRNA (**Figure S8C**). In a second experiment to determine the phenotype of organ specific cell populations transfected with **K-CART**, we intravenously administered Cy5-modified mRNA with **G-CART**/FLuc and **K-CART**/FLuc. Using flow cytometry, we analyzed single cell suspensions from the lung or spleen and found that the population of CART-transfected cells (Cy-5 positive cells) comprised ca. 38% B cells, 17%

endothelial cells, 6% CD3 T cells, 8% natural killer cells, 9% eosinophils, and 20% monocytes (**Figure S8B**).

K-CART effectively delivers siRNA to silence reporter gene expression in an in-vivo lung tumor model. As systemic administration of **K-CART**/FLuc results in preferential protein expression in the lung, we sought to assess whether this organ selectivity might be generalizable to other genetic polyanionic cargos, such as siRNA. The delivery and successful translation of mRNA elicits the intracellular expression of proteins, whereas the delivery of siRNA silences the translation of the mRNA for which it targets, resulting in the suppression of protein expression.³¹

As with mRNA, mixing siRNA and **K-CART** leads to similar nanoparticle formation. Characterization of the **K-CART**/siRNA particles reveals complete complexation of siRNA when formulated at a +/- charge ratio of 10:1 (>99% by Qubit RNA probe, **Figure S2**). DLS measurements of the **K-CART**/siRNA NPs reveal an initial diameter of 160 (+/- 2) nm which remains constant over two hours (**Figure S9**). The initial zeta potential of the particles is 32 (+/- 22) mV and, like the **K-CART**/mRNA NPs, **K-CART**/siRNA NPs retain a positive zeta potential over two hours (**Figure S10**). These comparisons suggest that the physical properties of the resulting CART/RNA NPs are not particularly sensitive to the exact nature or length of the RNA cargo. Additionally, in an MTT cellular proliferation assay, **K-CART**/siRNA NPs (like their mRNA-based congeners) also show no significant cell toxicity (**Figure S11**).

To assess the ability of CARTs to silence protein expression by siRNA delivery in vitro, we used an siRNA against FLuc (FLuc-siRNA) to decrease the expression of FLuc in stably FLuc-expressing LLC and 4T1 breast cancer cells (**Figure S4C**). We observed no silencing of FLuc expression in LLC cells when treated with **G-CART**/FLuc-siRNA but observed ca. 25% silencing when treated with **K-CART**/FLuc-siRNA. Conversely, in 4T1 breast cancer cells **G-CART**/FLuc-siRNA demonstrated greater knockdown efficacy than **K-CART**/FLuc-siRNA, 60% and 50% respectively. These results illustrate the complementary selectivities of the two CARTs, with **K-CART** performing better in Lewis lung carcinoma cells.

To assess siRNA knockdown in vivo, we first treated mice with **K-CART**/FLuc to establish FLuc expression in the lungs (see scheme in **Figure 5A**). Bioluminescence in the lung was clearly observed and quantified six hours after **K-CART**/FLuc injection. The mice were subsequently injected with either 10 ug siRNA against FLuc (**K-CART**/FLuc-siRNA) or 10 ug scrambled siRNA (**K-CART**/scrambled-siRNA, **Figure 5A**) and the FLuc bioluminescence was

measured after 18 hours. Mice treated with **K-CART**/FLuc-siRNA showed a 3-fold decrease in FLuc signal relative to that observed prior to siRNA administration and relative to that observed from administration of a scrambled siRNA or a PBS control (**Figure 5C**). IV administration of **K-CART**/FLuc-siRNA results in functional delivery of siRNA to the lungs, clearly disrupting expression of protein-encoding mRNA; thus, demonstrating that **K-CART**s are candidates to treat genetic disease in the lung via protein knock-down.

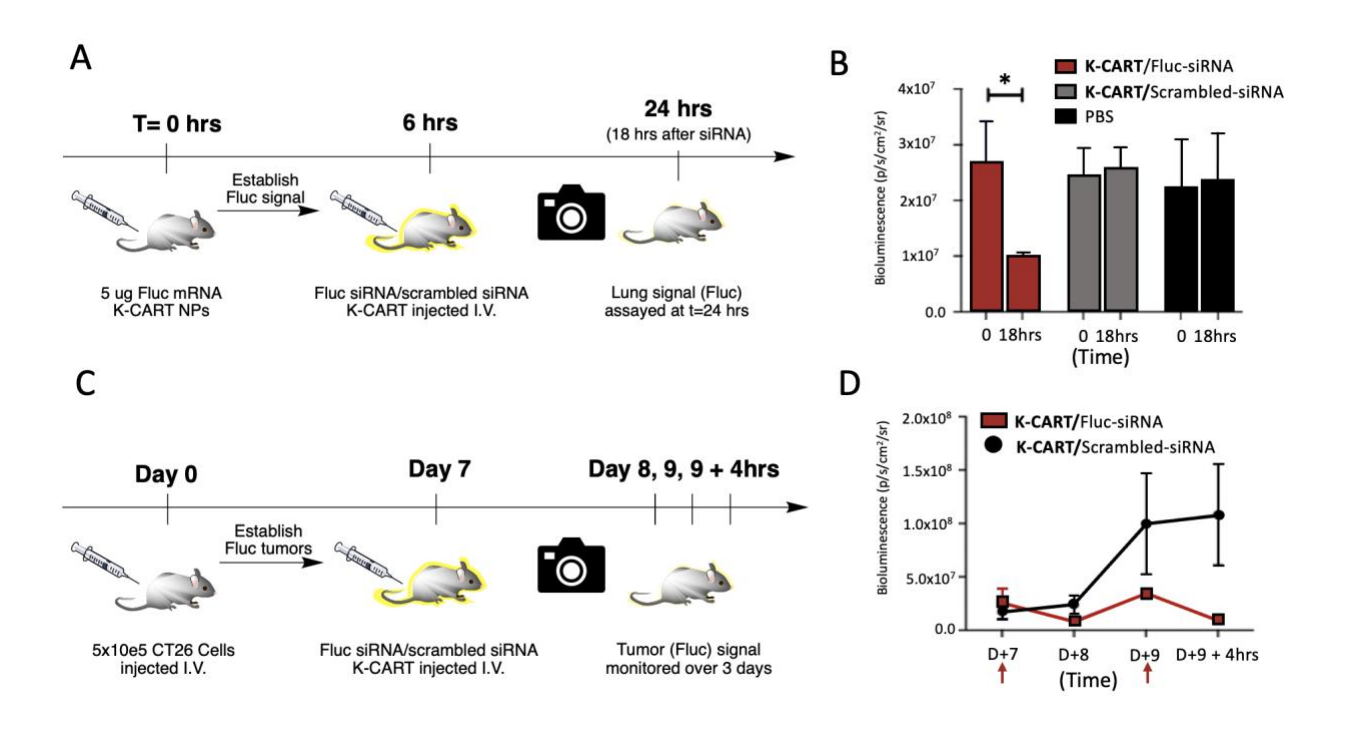


Figure 5 Silencing of FLuc protein expression in tumor cells in the lung with **K-CART**/FLuc-siRNA. A.) 5 ug FLuc mRNA was administered to mice. After 6 hours BLI was measured then 10 ug **K-CART**/FLuc-siRNA or **K-CART**/Scrambled-siRNA was administered IV the FLuc signal was assayed again at t=24 hours (18 hrs after siRNA). Group 1(red) received **K-CART**/FLuc-siRNA, Group 2 (grey) received scrambled **K-CART**/Scrambled-siRNA, Group 3 (black) received free FLuc siRNA B.) Measurement of BLI for siRNA treated vs control mice at T=24 hours compared to the levels at the time of administration of siRNA C.) 12 BALB/c mice were IV injected with 5x10⁵ FLuc expressing CT26 colon carcinoma cells. Group 1 (red) received two doses of 10 ug **K-CART**/FLuc-siRNA on day 7 and day 9 post tumor injection. Group 2 (black) received two doses of 10 ug control **K-CART**/Scrambled-siRNA on day 7 and day 9 post tumor injection D.) Measurement of BLI for siRNA treated mice was performed on day 7, 8, 9 and day 9+4 hrs. (arrows indicate injection timing) *Data representative of 2 indivudual experiments. Error bars are standard deviation, in panel D open symbols are used to indicate uncertainty, where not visible standard deviations are smaller than the symbol size. Significance was calculated using the two tailed T test with * p<0.01.\B\C/D.

To assess if CART mediated delivery of siRNA might be used to silence protein expression in cancer cells in the lung, we injected $5x10^5$ FLuc expressing CT26 colon carcinoma cells into 12 BALB/c mice IV into the tail vein; this procedure provides a means of establishing tumors selectively in the lung. After 7 days, bioluminescence imaging confirmed that FLuc-expressing tumors were selectively established in the lung (**Figure S12**). We then treated these mice twice in 48 hrs. using 10 ug of either **K-CART**/FLuc-siRNA or scrambled **K-CART**/Scrambled-siRNA (see scheme in **Figure 5C**). We observed a dramatic and significant reduction of FLuc signal from the mice treated with the **K-CART**/FLuc-siRNA (**Figure 5D**). These data indicate that **K-CART** is an excellent vehicle for siRNA delivery to and protein silencing of cells in the lung.

Discussion

Gene therapies provide promising new strategies to treat many canonically undruggable diseases. Emerging as a front-line nonviral candidate for gene delivery, ^{7, 26, 31} LNPs have been shown in early studies to enable delivery to and gene expression primarily in the liver. ⁵³ This has limited many clinical applications to therapeutic targets in the liver. It follows that an important goal in current nucleic acid delivery research would be the development of extrahepatic delivery systems that would broaden the clinical scope of mRNA therapy. A key to the realization of this goal is understanding factors that influence organ selectivity of LNPs and other gene delivery vectors.

CARTs present a nonviral delivery system with key distinctions from LNPs. In addition to their ability to undergo charge alteration through an O-to-N acyl shift, N-hydroxyethyl glycine-derived CARTs and serine-derived CARTs³⁹ exhibit selective transfection of the spleen^{10, 38, 43-44} rather than the liver. This is true even when the nature of the hydrophobic side chain of the CARTs is varied, though these chemical modifications do influence the types of cells which are transfected.⁴⁴ We now show that by changing the chemical structure of the cationic repeat unit from N-hydroxyethyl glycine (G-CART) or serine to N-hydroxyethyl lysine (K-CART) we see a marked shift from selective protein expression in the spleen to selective expression in the lung.

We demonstrate that **K-CART**s can achieve functional delivery of both mRNA and siRNA to the lung. Furthermore, by sequentially delivering mRNA and then siRNA for FLuc systemically in the same animal we observe first turn on of FLuc luminescence and then statistically significant reduction of FLuc luminescence, only in those animals that receive FLuc siRNA. While not

quantitative, these results show that regardless of the cargo (mRNA or siRNA) at least some of the same cells in the lung are transfected, indicating that the selectivity observed with these particles is influenced significantly by the CART vector. We further demonstrated that CARTs can functionally deliver siRNA to cancer cells in an established tumor within the lung.

To correlate the structure and properties of CARTs to their biological function, we investigated and compared the chemical behavior of homopolymers and amphiphilic CART oligomers derived from N-hydroxy glycine (**G-CART**) and N-hydroxy lysine (**K-CART**) cationic repeat units. The chemical structure of the α -amino ester segments in the amphiphilic CARTs has a significant influence on the chemical behavior of the oligomeric CART amphiphiles and their corresponding mRNA nanoparticles. The slower degradation kinetics of the dicationic lysine polymers (pH 6.5, $t_{1/2} = 12$ min) relative to the glycine analogs (pH 6.5, $t_{1/2} = 3$ min, **Figure S1**) is mirrored in the relative stability of their CART/mRNA nanoparticles in buffered aqueous solution (**Figure 3**). The introduction of a substituent at the alpha position of the amino ester both slows the rate of degradation and changes the mechanism; the cationic lysine polymers degrade by hydrolysis, whereas the glycine-derived polymers degrade predominantly by an O-to-N acyl shift to generate cyclic diketopiperazines.^{38, 41}

The differences in charge-altering kinetics of these cationic homopolymers are reflected in the dynamic and physical properties of the corresponding **K-CART**/mRNA and **G-CART**/mRNA NPs (**Figure 3**). The lysine-derived **K-CART**s form mRNA NPs with a hydrodynamic diameter of ~170 nm and a surface charge of +34 mV, which remain stable over the course of 2 hours at pH 7.4. For the **G-CART**/mRNA NPs,³⁸ the surface charge evolves from a positive zeta potential to a negative zeta potential over 20 minutes, and hydrodynamic diameter increases from 227 nm to ~450 nm over the course of one hour at pH 7.4.

The physical properties of many gene delivery agents have been shown to impact their circulation time and biodistribution. 15, 54-55, Previous studies 15-16, 33, 56-57 had implicated that the surface charge of the nanoparticle influences organ tropism. The selective organ targeting (SORT) approach 15 developed by Siegwart, *et al.* involves the engineering of LNPs to influence the tissue tropism of mRNA delivery by modulating, among other factors, the surface charge of the resulting particles. The differences in size, charge density, charge spatial array, and stability of the CART NPs (**Figure 3**) could contribute to the differential cell association and thus tissue tropism and selective cellular transfection relative to the **G-CART**/mRNA. Recent studies align with these

observations showing that systemic administration of highly cationic NP transfection agents are often correlated to functional delivery of mRNA to the lung, ^{15, 30, 34, 56-57} while anionic NP tend to exhibit protein expression in the spleen. ^{15-16, 30, 34} Indeed, **G-CART** NPs and serine-derived CART NPs, which both evolve over time to exhibit a negative surface potential, ³⁹ show selective RNA cargo expression in the spleen and **K-CART** NPs exhibiting stable cationic character show selective RNA cargo expression in the lung (**Figure 4**). The spleen-targeting **G-CART** ^{10, 38, 43} leads to highly effective delivery to monocytes and B cells. Notably, many of the cells transfected in vivo in the lung using **K-CART** are also immune system-related cells (e.g., B cells, monocytes, eosinophils, NK cells, T cells, neutrophils; **Figure S8B**). Importantly, treatment with **CART**/mRNAs shows no histological abnormalities in the major organs (i.e., brain, heart, kidney, liver, lung, and spleen; **Figure S5**). Thus, the CART methodology is a generalizable platform for selective, targeted mRNA delivery in vitro and in vivo, without recognizable adverse effects.

Despite recent advances in the development of non-viral gene delivery agents for extrahepatic delivery, the in vivo organ selectivity for mRNA delivery remains poorly understood. ^{26, 30-37, 45, 53, 58-60} **G-CART**/FLuc and **K-CART**/FLuc NPs, though lacking in any targeting ligands, show complementary and selective cellular transfection efficiencies in vitro and organ selective protein expression in vivo (**Figure 4**). Here we show that by altering the charge density and spatial distribution of cationic CART repeat units, either spleen or lungs can be targeted upon IV administration. It is possible that the surface charge of the **CART**/mRNA NPs can influence protein adsorption/opsonization upon injection into the blood stream. There is some evidence ^{15-16, 30, 32} that the composition of the resulting "protein corona," plays a critical role in the ultimate organ selectivity and retention of delivery vehicles. Further studies are underway to test this hypothesis and to correlate how the chemical structure of the CARTs influences the physical properties of the resulting CART/RNA NPs, the protein and cell surface interactions, and the cell/organ selectivity for CART/RNA delivery in vivo.

Conclusions

Nanoparticles that target particular diseased organs have the potential to transform gene therapy. Here we show that CART delivery technology can be used to target organs without the need of targeting ligands. Glycine-derived **G-CARTs** provide highly selective mRNA expression in the spleen (>99%) and the readily accessible (two steps) lysine-derived **K-CARTs** show

selective mRNA expression in the lung (~91%). Importantly, G-CART and K-CART induce no adverse effects in blood chemistries nor histopathological analysis of major organs. We further show that CARTs are effective for siRNA delivery: K-CARTs upon systemic administration, functionally deliver siRNA to the lung, efficiently suppressing reporter protein expression. We propose that this organ selectivity is related to functionality, density and spatial array of charges and lipids of the CART/mRNA NPs and their interactions with carriers and/or cell and organ surfaces. However, this and other hypotheses are an ongoing topic of study and part of further investigations on targeting other organs with new CART families. Critically, the G-CART and K-CART NPs were designed to exhibit different physical properties; K-CARTs are more highly cationic and compact, while G-CARTs acquire anionic character and change in size over time; and in turn exhibit different in vivo behavior and organ selective functional delivery. CARTs comprise a platform technology for the delivery of siRNA, mRNA, circRNA⁴² and DNA⁴⁰ in vitro and in vivo. The demonstration that CART delivery can now be selectively targeted to different organs based on differences in the intrinsic CART structural features opens new opportunities for their use in research and medicine.

Materials and methods

Reagents. Deuterated solvents (D₂O, CD₃OD, CDCl₃) were purchased from Cambridge Isotope Laboratories and used without further purification. THF, DCM, and toluene used for polymerization experiments were dried over activated 3 Å molecular sieves and used without further purification. Acetonitrile, methanol, toluene, DCM, and ethyl acetate used for the synthesis and purification of monomers and precursors were used without purification. Potassium hydride (KH), benzyl alcohol (BnOH), and trifluoroacetic acid (TFA) were purchased from Aldrich and used without purification. All other substrates were purchased from Fisher, Alfa Aesar, or Sigma Aldrich and used without further purification. Urea catalysts 1-(3,5-bis(trifluoromethyl)phenyl)-3-(3-(trifluoromethyl)phenyl) urea and 1-cyclohexyl-3-phenylurea were prepared as previously reported.⁵¹ Boc-morpholinone monomer and dodecyl carbonate monomer were prepared according to literature procedures.³⁸ BDK initiator and BDK G-CART were prepared as previously reported.⁴⁴ The 1-(3,5-bis-trifluoromethyl-phenyl)-3-cyclohexyl- thiourea used for some ring-opening polymerizations was prepared as previously reported.⁶¹ Ring-opening polymerization reactions were set up in a glovebox under nitrogen atmosphere and then performed

under nitrogen using air-free Schlenk techniques. Regenerated cellulose dialysis membranes (Spectra/Por 6 Standard RC; molecular weight cutoff 1,000) were purchased from Spectrum Laboratories, Inc. MTT was purchased from Fluka. EGFP mRNA (5meC, Ψ, L-6101), Cy5-EGFP mRNA (5meC, Ψ, L-6402), Fluc mRNA (5meC, Ψ, L-6107), and Cy5-Fluc mRNA (5meC, Ψ, L-7702), were purchased from TriLink BioTechnologies Inc. FLuc siRNA was purchased from Dharmacon (P-002099-01-20).

Cell lines. DC 2.4 cells, Lewis Lung Carcinoma (LLC) cells, HeLa cells, CT26 cells, 293T cells and 4T1 FLuc-expressing cells were cultured in RPMI 1640 medium (Invitrogen Life Technologies) supplemented with 10% heat-inactivated fetal calf serum (HyClone Laboratories), 100 U/mL penicillin, 100 ug/mL streptomycin (Invitrogen Life Technologies), as complete medium. All cells were grown at 37 °C in a 5% CO₂ atmosphere. Cells were passaged at ~80% confluence.

Mice. Female BALB/c mice (6-8 weeks old at treatment) and female C57Bl/6 mice (8-10 weeks old at treatment) were purchased from Charles River Laboratories. All mice were housed at the Comparative Medicine Pavilion at Stanford University.

Establishing stable FLuc expressing LLC and CT26 cell lines: Lentiviruses were produced using 293T cells co-transfected with the pCMV-VSV-G and the pCMV ΔR8.2 packaging plasmids (gift from Gozani lab, Stanford) and the pHIV-Luc-ZsGreen plasmid (pHIV-Luc-ZsGreen was a gift from Bryan Welm, Addgene plasmid # 39196). Transfection was performed using TransIT (Mirus Bio) as per the manufacturer instructions. Target cells were then incubated with the virus-containing supernatant for 24h. Transduced cells were then selected by two rounds of FACS sorting on ZsGreen expressing cells.

Instrumentation. ¹H-NMR and ¹³C-NMR spectra were recorded on either an Inova 300 MHz, Mercury 400 MHz, or Inova 500 MHz spectrometer. Gel permeation chromatography (GPC) was performed in tetrahydrofuran (THF) at a flow rate of 1.0 mL/min on a Shimadzu Prominence chromatograph equipped with two Jordi columns (Jordi DVB 1000 Å and DVB Mixed Bed Low) connected in series. A Wyatt Optilab TrEX differential refractive index detector and a miniDAWN TREOS2 3-angle analytical light scattering detector were employed, M_n (GPC) determined by comparison of elution time to a calibration curve of polystyrene standards. Particle size and zeta potential were measured using a Malvern Zetasizer Nano ZS90. Flow cytometry analysis was performed on a BD LSRII.UV FACS Analyzer (Stanford University Shared FACS Facility).

Bioluminescence was measured using a CCD camera (IVIS 100; Xenogen Corp.) or an AMI HT instrument and analyzed using Living Image Software (PerkinElmer) or alternatively, using a SpectraMax luminometer. For cell transfection phenotyping, a SpectraMax paradigm was used to measure BDK signal.

Synthesis N-(tert-butoxycarbonyl)-N-(2of MG 2a (methyl precursor hydroxyethyl)glycinate): A round-bottom flask was charged with glycine methyl ester HCl (270 mg, 2.2 mmol) and NaHCO₃ (500 mg, 6 mmol) in 60 mL acetonitrile. This mixture was refluxed for one hour at 85 °C, then bromoethanol (145 uL, 2.1 mmol) was added in one portion. The reaction was stirred overnight, filtered, then concentrated. This residue was resuspended in 4 mL MeOH and stirred for 5 minutes before adding di-tert-butyl dicarbonate in one portion (500 uL, 2.2 mmol). After stirring for 3 hours, the reaction was concentrated under reduced pressure to give 1.2 g white slurry as the crude product which was loaded onto silica gel and purified via flash chromatography using 2:1 DCM:EtOAc. Concentration of the relevant fractions yielded 182 mg clear residue (0.87 mmol, 40% yield). The ¹H NMR of the isolated product matched that reported in the literature.⁴¹

Synthesis of M_G monomer 3a (tert-butyl 2-oxomorpholine-4-carboxylate): The linear alcohol intermediate 2a (81 mg, 0.38 mmol) along with catalytic p-toluenesulfonic acid (12 mg) was dissolved in 15 mL toluene and refluxed (110 °C), monitoring reaction progress by TLC (9:1 DCM: EtOAc). After a total of 30 minutes, the reaction was cooled to room temperature and concentrated under reduced pressure. The crude mixture was loaded onto silica gel and purified via flash chromatography using 9:1 DCM:EtOAc. Concentration of the relevant fractions yielded 64 mg clear residue (0.31 mmol, 84% yield). NMR matched that reported in the literature.⁴¹

Overall yield for 2-steps = 34 % yield

2b (methyl N^2 , N^6 -bis(tert-butoxycarbonyl)- N^2 -(2-**Synthesis** of M_K precursor **hydroxyethyl)lysinate):** A round-bottom flask was charged with N-epsilon-Boc-L-Lysine methyl ester HCl (1.18g, 4 mmol) and NaHCO₃ (750 mg, 8.9 mmol) in 12 mL acetonitrile. This mixture was refluxed for one hour at 85 °C, then bromoethanol (300 uL, 4.4 mmol) was added in one portion. The reaction was stirred overnight, filtered, and then concentrated. This residue was resuspended in 4 mL MeOH and stirred for 5 minutes before adding di-tert-butyl dicarbonate in one portion (950 uL, 4.15 mmol). After stirring overnight, the reaction was concentrated under reduced pressure to give 1.7 g yellow residue as the crude product which was loaded onto silica

gel and purified via flash chromatography using 2:1 DCM:EtOAc. Concentration of the relevant fractions yielded 857 mg clear residue (2.12 mmol, 53% yield). NMR spectra and characterization data provided in the supporting information.

Synthesis of M_K **monomer 3b:** (*tert*-butyl 3-(4-((*tert*-butoxycarbonyl)amino)butyl)-2-oxomorpholine-4-carboxylate): The linear alcohol intermediate **2b** (140 mg, 0.35 mmol) along with catalytic *p*-toluenesulfonic acid (10 mg) was taken up in 15 mL toluene and refluxed (110 °C), monitoring reaction progress by TLC (9:1 DCM: EtOAc). After a total of 20 minutes, the reaction was cooled to room temperature and concentrated under reduced pressure. The crude mixture was loaded onto silica gel and purified via flash chromatography using 9:1 DCM:EtOAc. Concentration of the relevant fractions yielded 115 mg clear residue (0.31 mmol, 89% yield).

Overall yield for 2-steps = 47 % yield. NMR spectra and characterization data provided in the supporting information.

Synthesis of homopolymer p(heK): A flame-dried vial was loaded with M_K (38.5 mg, 0.103 mmol, 54 eq) in 75 uL THF. To this solution was added a mixture of KH (0.04 mg, 0.001 mmol, 1 eq), BnOH (0.2 mg, 0.002 mmol, 2 eq), and 1-cyclohexyl-3-phenylurea (1.3 mg, 0.006 mmol, 6 eq) in 25 uL THF. After stirring at R.T. for 30 s, the reaction mixture was submerged in an acetone/dry ice bath at -78 °C. The reaction was allowed to stir for 20 minutes, then quenched with 5 uL AcOH in 100 uL THF. After quenching the reaction at -78 °C for 2 minutes, the solution was warmed to room temperature. The product was then dialyzed in DCM/MeOH overnight (1 kDa dialysis tubing). Concentration of dialyzed polymer 1 yielded 31.5 mg clear residue (81 % yield). NMR spectra and characterization data provided in the supporting information.

Synthesis of Boc-K-CART: A flame dried vial loaded with dodecyl carbonate monomer (16.5 mg, 0.05 mmol) and was stirred in 50 uL THF at room temperature for 5 minutes to homogenize the reactants. To this starting material was added a solution of KH (0.2 mg, 0.005 mmol), 1-cyclohexyl-3-phenylurea (3.3 mg, 0.015 mmol) and BnOH (0.54 mg, 0.005 mmol) in 25 uL THF. After stirring at R.T. for 2 minutes, M_K (37 mg, 0.1 mmol) in 50 uL THF was added and reaction was submerged in an acetone/dry ice bath. The reaction was allowed to stir at -78 °C for 20 minutes, then quenched with 5 uL AcOH in 100 uL THF. After stirring the quenched reaction at -78 °C for 2 minutes, the reaction was warmed to room temperature and analyzed for conversion by 1 H NMR. The product was then dialyzed in DCM/MeOH overnight (1 kDa dialysis bag).

Concentration of the recovered polymer yielded 24 mg of a clear residue (45% yield). NMR spectra and characterization data provided in the supporting information.

Synthesis of BDK Boc-K-CART: A flame dried vial loaded with dodecyl carbonate (32.5 mg, 0.1 mmol) and BDK initiator (2.4 mg, 0.0072 mmol) was stirred in 40 uL THF at room temperature. To this mixture was added a solution of KH (0.6 mg, 0.015 mmol), and 1-(3,5-bis(trifluoromethyl)phenyl)-3-(3-(trifluoromethyl)phenyl) urea (10 mg, 0.045 mmol). The reaction was stirred for 1 minute, then M_K was added to the reaction as a solid (45 mg, 0.12 mmol). The reaction was allowed to stir for 3-5 minutes until all M_K had dissolved, then submerged in an acetone/dry ice bath. The reaction was allowed to stir at -78 C for 45 minutes, then quenched with 5 uL AcOH in 100 uL THF. After stirring the quenched reaction at -78 C for 2 minutes, the reaction was warmed to room temperature and was then dialyzed in DCM/MeOH overnight (1 kDa dialysis bag). Concentration of the recovered polymer yielded 32 mg clear residue (40% yield). NMR spectra and characterization data provided in the supporting information.

Deprotection of p(heK) to the oligocation p(heK)²⁺: p(heK) polymer (30 mg) was dissolved in 3 mL DCM. To this solution was added 0.3 mL TFA and allowed to stir under N₂. After 4 hours, the reaction was concentrated, yielding 33 mg of a foamy tan residue. NMR spectra and characterization data provided in the supporting information.

Deprotection of Boc-K-CART to yield K-CART (D:Lys 14:8): Boc-K-CART (35 mg) polymer was dissolved in DCM (3.5 mL). To this solution was added TFA (0.35 mL) and allowed to stir under N₂. After 4 hours, the reaction was concentrated, yielding 36 mg of a foamy tan residue. NMR spectra and characterization data provided in the supporting information.

Deprotection of BDK Boc-K-CART to yield BDK K-CART (D:Lys 13:5.5): BDK Boc-K-CART (25 mg) polymer was dissolved in DCM (2.5 mL). To this solution was added TFA (0.25 mL) and allowed to stir under N₂. After 4 hours, the reaction was concentrated, yielding 26 mg of a foamy tan residue. NMR spectra and characterization data provided in the supporting information.

Procedure for comparative degradation kinetics experiment in D₂O: Deprotected polymer (10.4 mg, 0.048 mmol by repeat units) was dissolved in 500 uL D₂O with 7 mg sodium toluenesulfonate as internal standard (0.036 mmol; δ 2.38). The t_0 ¹H NMR spectrum was acquired with the parameters (Varian) nt = 8, at = 8, and d1 = 12, which were confirmed to provide a long enough time between scans to ensure accurate relative integrations. 500 uL of the 3.3 M

(HK₂PO₄/H₂KPO₄) buffer solution in D₂O was then added to the NMR tube, which was inverted multiple times to ensure thorough mixing. NMR spectra were then acquired once every 90 s for 2.5 h using the parameters nt = 4, at = 8, and d1 = 12. The arrayed spectral data were analyzed using MNova software. This method and additional details and NMR regarding the degradation of $p(heG)^+$ have been published elsewhere, ⁴¹ representative NMR spectra from the degradation of $p(heK)^{2+}$ provided in the supporting information (Figure S13).

CART-mRNA/siRNA NP formulation: Representative procedure. To 21.0 uL of RNAse free PBS (pH 5.5) was added 2.1 uL of a 0.2 ug/uL solution of FLuc mRNA. To this solution was added 0.40 uL of 2 mM **K-CART** (stored in DMSO). The solution was mixed for 20 seconds and used in vitro or in vivo immediately following formulation.

CART NP size measurements: Sizing measurements were performed using a Malvern Zetasizer Nano ZS90: A volume of CART to achieve a 10:1 +/- ratio was mixed into a solution containing 6.3 uL of a 0.2 ug/uL solution of SEAP mRNA or siRNA, and 17.1 uL pH 5.5 PBS. This mixture was incubated for 30 s at room temperature, then added to a cuvette containing 100 uL RPMI media (-phenol red). Measurements were taken at the indicated times and the sizes reported are the Z-averages of measurements run in triplicate with error expressed as ±SD.

CART NP zeta potential measurements: Zeta potential measurements were performed using a Malvern Zetasizer Nano ZS90: A volume of CART to achieve a 10:1 +/- ratio was mixed into a solution containing 5.0 uL of a 0.2 ug/uL solution of SEAP mRNA or siRNA, 14.0 uL pH 5.5 PBS, then incubated for 30s at room temperature. 5 uL of this solution was added to a zeta potential cuvette containing 795 uL DI water. Measurements were taken at the indicated times and reported are the average voltages of measurements run in triplicate with error expressed as ±SD.

RNA percent Encapsulation Determination by Qubit Probe: Encapsulation efficiency was measured by the fluorescence of the RNA-specific Qubit RNA HS dye (Q32852; Invitrogen). Briefly, mRNA or siRNA was complexed with K-CART as described above using 420 ng of RNA and enough CART for a net 10:1 (cation:anion) ratio. This was added to 0.75 mL of RNasefree deionized water containing 5 uL of Qubit reagent. The fluorescence of the solution was immediately measuring using an excitation wavelength of 630 (4-nm slit width) and emission wavelength of 680 nm (5-nm slit width). Percent encapsulation was determined by subtracting the fluorescence of the Qubit dye alone (no RNA) and normalizing to the fluorescence of Qubit with uncomplexed RNA.

In vitro cellular transfection: One day before transfection, cells were plated at 40,000 cells per well in a 96 well plate. On the day of transfection, complete media was replaced with $100 \,\mu$ l serumfree RPMI. FLuc mRNA (TriLink) or FLuc siRNA (dharmacon) was formulated with CART in a 10:1 +/- ratio, mixed for 20 s, then $2 \,\mu$ l of the mixture was added to the cells (1 ng/1000 cells). After four hours, $5 \,\mu$ l of PBS containing 3 mg/ml of luciferin was added to each well and the luminescent signal was measured using a SpectraMax L luminometer.

MTT Viability Assay: Cellular viability following treatment with CART–mRNA or CART-siRNA complexes was assayed using a standard MTT/formazan turnover assay. Briefly, HeLa, DC 2.4 and LLC cells were seeded at 5000 cells per well, then treated with CART–RNA complexes at a dose of 5 ng (1 ng/1000 cells). Cells were grown for 3 d, after which time 10 uL of PBS containing 2 uL of a 5 mg/mL solution of MTT (Fluka) was added to each well. Cells were incubated for an additional 3 h then the media was removed and 100 μl DMSO was added to each well. Cells were mixed for 15 min at 37°C and then absorbance was measured at 540 nm.

In vitro siRNA FLuc knockdown: In vitro silencing of FLuc reporter gene in LLC and 4T-1 stably-FLuc expressing cells. 10⁵ FLuc-expressing cells were treated with 200ng FLuc-targeting siRNA formulated in **G-CART**, **K-CART**, or PBS as described above. Bioluminescence was quantified 24hrs post treatment. Untreated cells were included as a control.

Live animal studies. Experimental protocols were approved by the Stanford Administrative Panel on Laboratory Animal Care and were performed in accordance with all national or local guidelines and regulations.

In Vivo transfection of Fluc mRNA. CART—mRNA NPs were prepared as described above using 5 ug mRNA per mouse in a total volume of 100 uL. Complexes were mixed for 20 s before IV injection into the tail vein of female BALB/c mice. After 8 h, 150 mg/kg D-luciferin was injected i.p. and mice were anesthetized with isoflurane for 5 minutes. Luminescence was measured using an AMI Imaging System CCD camera (AMI HT), and analyzed using AMI View software or alternatively using the IVIS 100 (Xenogen Corp.) imaging system equipped with a cooled charge-coupled device camera and analyzed using Living Image software. For bioluminescent imaging of excised organs, mice were sacrificed 5 minutes after the whole-body imaging, then individual organs were harvested and imaged within 5 minutes after sacrifice, all measurements were averages of groups of three animals.

Flow Cytometry method for phenotyping of transfected cells in the lung and spleen: To phenotype CART-transfected cell populations, we used BDK labeled **K-CART**, BDK labeled **G-CART** or Cy5.5 labeled eGFP mRNA (TriLink). 45 min post transfection mice were sacrificed, and lungs and spleens were harvested. Single cell suspensions of splenocytes were prepared by homogenizing and filtering spleens. Next, red blood cells were lysed for 10 min in ACK lysis buffer. Single cell suspension of the lung was prepared by cutting the lung into tiny pieces and incubating it in PBS containing 1mg/ml collagenase for 20 min at 37°C. Cells were stained using panel 1: CD45 FITC, CD31 PE, EpCam PerCP Cy5.5, CD11b BV605, CD3 BV786 and panel 2: CD11c PE-Cy7, CD64 PE, IA/IE Ax488, CD24 PerCP, CD11b BV605, CD49b eF450. Flow cytometry analysis was performed using a LSRII (BD).

In vivo silencing of FLuc transfected cells. First, mice were injected with 5 ug FLuc mRNA formulated with K-CART. Six hours post injection, bioluminescence was measured before the animals were injected with either 10 ug FLuc siRNA K-CART or 10 ug scrambled siRNA K-CART. At 18 hours post siRNA mRNA injection mice were imaged again using an AMI HT.

Tumor implantation and siRNA treatment. 5×10^6 CT26 FLuc cells were injected intravenously in BALB/c mice. On day 7, tumor establishment was confirmed by bioluminescence imaging using an AMI HT. Treatments were given on day 7 and 9 after tumor injection. For each treatment, mice were injected IV. with 10 ug FLuc or control siRNA formulated with **K-CART** at a 10:1 +/- ratio in 100 μ l of PBS pH 5.5. Tumor growth was monitored by bioluminescence.

Histology and Hematology. K-CART/mRNA NPs were prepared as described above using 5 ug mRNA per mouse in a total volume of 100 uL. Complexes were mixed for 20 s before IV injection into the tail vein of female BALB/c mice. After 72 hours, following humane euthanasia, tissues were fixed by immersion in 10% neutral buffered formalin. Tissues were then processed, embedded in paraffin, sectioned at 5.0mm, and routinely stained with hematoxylin and eosin (H&E). Stained sections were evaluated blindly by a board-certified veterinary pathologist using an Olympus BX43 brightfield microscope. Photomicrographs were captured using an Olympus DP27 digital camera and the Olympus cellSens software. Representative images presented in Figure S5. Complete blood count and serum chemistry levels for the treated group were within normal range.

ASSOCIATED CONTENT

Supporting Information

Supporting Information is available free of charge at

NMR spectra and characterization of materials; synthesis of homo-p(he-X) polymers and their kinetics of degradation in Figure S1; percent encapsulation of RNA in Figure S2; representative DLS size distribution plot of **K-CART**/mRNA in Figure S3; efficacy and cellular uptake in Figure S4; histo-pathological assessment of mouse tissues and blood in Figure S5; representative organ BLI of mice sacrificed 8 hours after mRNA delivery with **K-CART**/FLuc mRNA in Figure S6; structure of BDK-K-CART in Figure S7; flow cytometry data in Figure S8; additional DLS and zeta potential data in Figures S9 and S10; assessment of cell viability by MTT assay in Figures S4 and S11; representative luminescence images of mice harboring lung metastases of CT26-FLuc colon carcinomas in Figure S12; representative NMR spectra from the degradation of **p(heK)**²⁺ in Figure S13.

AUTHOR INFORMATION

Corresponding Author

Robert M. Waymouth, Department of Chemistry, Stanford University, Stanford CA 94305, United States; orcid.org/0000-0001-9862-9509

Authors

Paul A. Wender Department of Chemistry, Stanford University, Stanford CA 94305, United States; Department of Chemical and Systems Biology, Stanford University, Stanford CA 94305, United States

Timothy R. Blake Department of Chemistry, Stanford University, Stanford CA 94305, United States; orcid.org/0000-0001-7548-1492

Rebecca L. McClellan Department of Chemistry, Stanford University, Stanford CA 94305, United States

Trevor J. Del Castillo Department of Chemistry, Stanford University, Stanford CA 94305, United States; orcid.org/0000-0001-5120-1935

Wilson C. Ho Department of Chemistry, Stanford University, Stanford CA 94305, United States; orcid.org/0000-0002-1322-7728

Ronald Levy Division of Oncology, Department of Medicine, Stanford Cancer Institute, Stanford University, Stanford CA 94305, United States

Ole A. W. Haabeth Division of Oncology, Department of Medicine, Stanford Cancer Institute, Stanford University, Stanford CA 94305, United States; orcid.org/0000-0002-1153-9250

Adrienne Sallets Division of Oncology, Department of Medicine, Stanford Cancer Institute, Stanford University, Stanford CA 94305, United States

Jose G. Vilches-Moure Department of Comparative Medicine, Stanford Cancer Institute, Stanford University, Stanford CA 94305, United States

Author Contributions

Tim. R. Blake and Ole A.W. Haabeth contributed equally to this work. The article was written through contributions of all authors. All authors have given approval to the final version of the article

Notes

The authors declare the following competing financial interest(s): Ronald Levy serves on the Scientific Advisory Boards of Quadriga, BeiGene, GigaGen, Teneobio, Nurix, Dragonfly, Apexigen, Viracta, Spotlight, Immunocore, Walking Fish, Kira, Abintus Bio, Khloris, Virsti, BiolineRx. Paul Wender serves on the Science Advisory Boards of BryoLogyx, N1 Life, Synaptogenix, SuperTrans Medical, Vault Pharma, and Cytokinetics. The other authors have no conflicts of interest to declare.

Acknowledgements

This work was supported by grants 5R01CA245533-03 (R.M.W., P.A.W., R.L.), R01 CA031845 (P.A.W.), F32GM133150 (T.J.D.C.) from the National Institute of Health, grants CHE-2002933 (to R.M.W.) and CHE-848280 (P.A.W) from the National Science Foundation; the Child Health Research Institute at Stanford University and the SPARK Translational Research Program in the Stanford University School of Medicine (R.M.W., P.A.W., R.L.). Support through the Stanford Cancer Translational Nanotechnology Training T32 Training Grant T32 CA196585 funded by the National Cancer Institute (T.R.B) and through the Center for Molecular Analysis and Design at Stanford University (R.L.M) is also acknowledged. Part of this work was performed at the Stanford Nano Shared Facilities (SNSF), supported by the National Science Foundation under award ECCS-2026822.

Received: ((will be filled in by the editorial staff))

Revised: ((will be filled in by the editorial staff))

Published online: ((will be filled in by the editorial staff))

References

- 1. Baden, L. R.; El Sahly, H. M.; Essink, B.; Kotloff, K.; Frey, S.; Novak, R.; Diemert, D.; Spector, S. A.; Rouphael, N.; Creech, C. B., et al. Efficacy and Safety of the mRNA-1273 SARS-CoV-2 Vaccine. *N Engl J Med* **2021**, *384* (5), 403-416.
- 2. Batty, C. J.; Heise, M. T.; Bachelder, E. M.; Ainslie, K. M. Vaccine formulations in clinical development for the prevention of severe acute respiratory syndrome coronavirus 2 infection. *Adv Drug Deliv Rev* **2021**, *169*, 168-189.
- 3. Buschmann, M. D.; Carrasco, M. J.; Alishetty, S.; Paige, M.; Alameh, M. G.; Weissman, D. Nanomaterial Delivery Systems for mRNA Vaccines. *Vaccines (Basel)* **2021**, *9* (1), 65.
- 4. Meyer, M.; Huang, E.; Yuzhakov, O.; Ramanathan, P.; Ciaramella, G.; Bukreyev, A. Modified mRNA-Based Vaccines Elicit Robust Immune Responses and Protect Guinea Pigs From Ebola Virus Disease. *J Infect Dis* **2018**, *217* (3), 451-455.
- 5. Pardi, N.; Hogan, M. J.; Pelc, R. S.; Muramatsu, H.; Andersen, H.; DeMaso, C. R.; Dowd, K. A.; Sutherland, L. L.; Scearce, R. M.; Parks, R., et al. Zika virus protection by a single low-dose nucleoside-modified mRNA vaccination. *Nature* **2017**, *543* (7644), 248-251.
- 6. Polack, F. P.; Thomas, S. J.; Kitchin, N.; Absalon, J.; Gurtman, A.; Lockhart, S.; Perez, J. L.; Perez Marc, G.; Moreira, E. D.; Zerbini, C., et al. Safety and Efficacy of the BNT162b2 mRNA Covid-19 Vaccine. *N Engl J Med* **2020**, *383* (27), 2603-2615.
- 7. Kyriakidis, N. C.; Lopez-Cortes, A.; Gonzalez, E. V.; Grimaldos, A. B.; Prado, E. O. SARS-CoV-2 vaccines strategies: a comprehensive review of phase 3 candidates. *NPJ Vaccines* **2021**, *6* (1), 28.
- 8. Fenton, O. S.; Olafson, K. N.; Pillai, P. S.; Mitchell, M. J.; Langer, R. Advances in Biomaterials for Drug Delivery. *Adv Mater* **2018**, e1705328.
- 9. Ramaswamy, S.; Tonnu, N.; Tachikawa, K.; Limphong, P.; Vega, J. B.; Karmali, P. P.; Chivukula, P.; Verma, I. M. Systemic delivery of factor IX messenger RNA for protein replacement therapy. *Proc Natl Acad Sci U S A* **2017**, *114* (10), E1941-E1950.
- 10. Haabeth, O. A. W.; Blake, T. R.; McKinlay, C. J.; Waymouth, R. M.; Wender, P. A.; Levy, R. mRNA vaccination with charge-altering releasable transporters elicits human T cell responses and cures established tumors in mice. *Proc Natl Acad Sci U S A* **2018**, *115* (39), E9153-E9161.
- 11. Miller, J. B.; Siegwart, D. J. Design of synthetic materials for intracellular delivery of RNAs: From siRNA-mediated gene silencing to CRISPR/Cas gene editing. *Nano Research* **2018**, *11* (10), 5310-5337.
- 12. Oberli, M. A.; Reichmuth, A. M.; Dorkin, J. R.; Mitchell, M. J.; Fenton, O. S.; Jaklenec, A.; Anderson, D. G.; Langer, R.; Blankschtein, D. Lipid Nanoparticle Assisted mRNA Delivery for Potent Cancer Immunotherapy. *Nano Lett* **2017**, *17* (3), 1326-1335.
- 13. Sahin, U.; Derhovanessian, E.; Miller, M.; Kloke, B. P.; Simon, P.; Lower, M.; Bukur, V.; Tadmor, A. D.; Luxemburger, U.; Schrors, B., et al. Personalized RNA mutanome vaccines mobilize poly-specific therapeutic immunity against cancer. *Nature* **2017**, *547* (7662), 222-226.
- 14. Van Lint, S.; Renmans, D.; Broos, K.; Dewitte, H.; Lentacker, I.; Heirman, C.; Breckpot, K.; Thielemans, K. The ReNAissanCe of mRNA-based cancer therapy. *Expert Review of Vaccines* **2015**, *14* (2), 235-251.
- 15. Cheng, Q.; Wei, T.; Farbiak, L.; Johnson, L. T.; Dilliard, S. A.; Siegwart, D. J. Selective organ targeting (SORT) nanoparticles for tissue-specific mRNA delivery and CRISPR-Cas gene editing. *Nat Nanotechnol* **2020**, *15* (4), 313-320.

- 16. Kranz, L. M.; Diken, M.; Haas, H.; Kreiter, S.; Loquai, C.; Reuter, K. C.; Meng, M.; Fritz, D.; Vascotto, F.; Hefesha, H., et al. Systemic RNA delivery to dendritic cells exploits antiviral defence for cancer immunotherapy. *Nature* **2016**, *534* (7607), 396-401.
- 17. Li, S.-D.; Huang, L. Pharmacokinetics and Biodistribution of Nanoparticles. *Molecular Pharmaceutics* **2008**, *5* (4), 496-504.
- 18. Venkataraman, S.; Hedrick, J. L.; Ong, Z. Y.; Yang, C.; Ee, P. L.; Hammond, P. T.; Yang, Y. Y. The effects of polymeric nanostructure shape on drug delivery. *Adv Drug Deliv Rev* **2011**, *63* (14-15), 1228-46.
- 19. Keil, T. W. M.; Baldassi, D.; Merkel, O. M. T-cell targeted pulmonary siRNA delivery for the treatment of asthma. *Wiley Interdiscip Rev Nanomed Nanobiotechnol* **2020**, *12* (5), e1634.
- 20. Griesenbach, U.; Alton, E. W. Moving forward: cystic fibrosis gene therapy. *Hum Mol Genet* **2013**, *22* (R1), R52-8.
- 21. Samaridou, E.; Heyes, J.; Lutwyche, P. Lipid nanoparticles for nucleic acid delivery: Current perspectives. *Adv Drug Deliv Rev* **2020**, *154-155*, 37-63.
- 22. Haabeth, O. A. W.; Blake, T. R.; McKinlay, C. J.; Tveita, A. A.; Sallets, A.; Waymouth, R. M.; Wender, P. A.; Levy, R. Local Delivery of Ox40l, Cd80, and Cd86 mRNA Kindles Global Anticancer Immunity. *Cancer Res* **2019**, *79* (7), 1624-1634.
- 23. Hewitt, S. L.; Bai, A.; Bailey, D.; Ichikawa, K.; Zielinski, J.; Karp, R.; Apte, A.; Arnold, K.; Zacharek, S. J.; Iliou, M. S., et al. Durable anticancer immunity from intratumoral administration of IL-23, IL-36γ, and OX40L mRNAs. *Science Translational Medicine* **2019**, *11* (477), eaat9143.
- 24. Miyazaki, T.; Uchida, S.; Nagatoishi, S.; Koji, K.; Hong, T.; Fukushima, S.; Tsumoto, K.; Ishihara, K.; Kataoka, K.; Cabral, H. Polymeric Nanocarriers with Controlled Chain Flexibility Boost mRNA Delivery In Vivo through Enhanced Structural Fastening. *Adv Healthc Mater* **2020**, *9* (16), e2000538.
- 25. Frank, A. M.; Buchholz, C. J. Surface-Engineered Lentiviral Vectors for Selective Gene Transfer into Subtypes of Lymphocytes. *Mol Ther Methods Clin Dev* **2019**, *12*, 19-31.
- 26. Lee, J.; Kim, D.; Byun, J.; Wu, Y.; Park, J.; Oh, Y. K. In vivo fate and intracellular trafficking of vaccine delivery systems. *Adv Drug Deliv Rev* **2022**, *186*, 114325.
- 27. Li, Q.; Chan, C.; Peterson, N.; Hanna, R. N.; Alfaro, A.; Allen, K. L.; Wu, H.; Dall'Acqua, W. F.; Borrok, M. J.; Santos, J. L. Engineering Caveolae-Targeted Lipid Nanoparticles To Deliver mRNA to the Lungs. *ACS Chem Biol* **2020**, *15* (4), 830-836.
- 28. Tanaka, H.; Sakurai, Y.; Anindita, J.; Akita, H. Development of lipid-like materials for RNA delivery based on intracellular environment-responsive membrane destabilization and spontaneous collapse. *Adv Drug Deliv Rev* **2020**, *154-155*, 210-226.
- 29. Kusumoto, K.; Akita, H.; Ishitsuka, T.; Matsumoto, Y.; Nomoto, T.; Furukawa, R.; El-Sayed, A.; Hatakeyama, H.; Kajimoto, K.; Yamada, Y., et al. Lipid Envelope-Type Nanoparticle Incorporating a Multifunctional Peptide for Systemic siRNA Delivery to the Pulmonary Endothelium. *ACS Nano* **2013**, *7* (9), 7534-7541.
- 30. Dilliard, S. A.; Cheng, Q.; Siegwart, D. J. On the mechanism of tissue-specific mRNA delivery by selective organ targeting nanoparticles. *Proc Natl Acad Sci U S A* **2021**, *118* (52).
- 31. Kumar, R.; Santa Chalarca, C. F.; Bockman, M. R.; Bruggen, C. V.; Grimme, C. J.; Dalal, R. J.; Hanson, M. G.; Hexum, J. K.; Reineke, T. M. Polymeric Delivery of Therapeutic Nucleic Acids. *Chem Rev* **2021**, *121* (18), 11527-11652.

- 32. Qiu, M.; Tang, Y.; Chen, J.; Muriph, R.; Ye, Z.; Huang, C.; Evans, J.; Henske, E. P.; Xu, Q. Lung-selective mRNA delivery of synthetic lipid nanoparticles for the treatment of pulmonary lymphangioleiomyomatosis. *Proc Natl Acad Sci U S A* **2022**, *119* (8).
- 33. Wei, T.; Cheng, Q.; Farbiak, L.; Anderson, D. G.; Langer, R.; Siegwart, D. J. Delivery of Tissue-Targeted Scalpels: Opportunities and Challenges for In Vivo CRISPR/Cas-Based Genome Editing. *ACS Nano* **2020**, *14* (8), 9243-9262.
- 34. Zhang, D.; Atochina-Vasserman, E. N.; Maurya, D. S.; Liu, M.; Xiao, Q.; Lu, J.; Lauri, G.; Ona, N.; Reagan, E. K.; Ni, H., et al. Targeted Delivery of mRNA with One-Component Ionizable Amphiphilic Janus Dendrimers. *J Am Chem Soc* **2021**, *143* (43), 17975-17982.
- 35. Abd Elwakil, M. M.; Khalil, I. A.; Elewa, Y. H. A.; Kusumoto, K.; Sato, Y.; Shobaki, N.; Kon, Y.; Harashima, H. Lung-Endothelium-Targeted Nanoparticles Based on a pH-Sensitive Lipid and the GALA Peptide Enable Robust Gene Silencing and the Regression of Metastatic Lung Cancer. *Advanced Functional Materials* **2019**, *29* (18), 1807677.
- 36. Karlsson, J.; Tzeng, S. Y.; Hemmati, S.; Luly, K. M.; Choi, O.; Rui, Y.; Wilson, D. R.; Kozielski, K. L.; Quinones-Hinojosa, A.; Green, J. J. Photocrosslinked Bioreducible Polymeric Nanoparticles for Enhanced Systemic siRNA Delivery as Cancer Therapy. *Adv Funct Mater* **2021**, *31* (17).
- 37. Abd Elwakil, M. M.; Gao, T.; Isono, T.; Sato, Y.; Elewa, Y. H. A.; Satoh, T.; Harashima, H. Engineered epsilon-decalactone lipomers bypass the liver to selectively in vivo deliver mRNA to the lungs without targeting ligands. *Mater Horiz* **2021**, *8* (8), 2251-2259.
- 38. McKinlay, C. J.; Vargas, J. R.; Blake, T. R.; Hardy, J. W.; Kanada, M.; Contag, C. H.; Wender, P. A.; Waymouth, R. M. Charge-altering releasable transporters (CARTs) for the delivery and release of mRNA in living animals. *Proc Natl Acad Sci U S A* **2017**, *114* (4), E448-E456.
- 39. Benner, N. L.; McClellan, R. L.; Turlington, C. R.; Haabeth, O. A. W.; Waymouth, R. M.; Wender, P. A. Oligo(serine ester) Charge-Altering Releasable Transporters: Organocatalytic Ring-Opening Polymerization and their Use for in Vitro and in Vivo mRNA Delivery. *J Am Chem Soc* **2019**, *141* (21), 8416-8421.
- 40. Benner, N. L.; Near, K. E.; Bachmann, M. H.; Contag, C. H.; Waymouth, R. M.; Wender, P. A. Functional DNA Delivery Enabled by Lipid-Modified Charge-Altering Releasable Transporters (CARTs). *Biomacromolecules* **2018**, *19* (7), 2812-2824.
- 41. Blake, T. R.; Ho, W. C.; Turlington, C. R.; Zang, X.; Huttner, M. A.; Wender, P. A.; Waymouth, R. M. Synthesis and mechanistic investigations of pH-responsive cationic poly(aminoester)s. *Chem Sci* **2020**, *11* (11), 2951-2966.
- 42. Chen, R.; Wang, S. K.; Belk, J. A.; Amaya, L.; Li, Z.; Cardenas, A.; Abe, B. T.; Chen, C. K.; Wender, P. A.; Chang, H. Y. Engineering circular RNA for enhanced protein production. *Nat Biotechnol* **2022**.
- 43. Haabeth, O. A. W.; Lohmeyer, J. J. K.; Sallets, A.; Blake, T. R.; Sagiv-Barfi, I.; Czerwinski, D. K.; McCarthy, B.; Powell, A. E.; Wender, P. A.; Waymouth, R. M., et al. An mRNA SARS-CoV-2 Vaccine Employing Charge-Altering Releasable Transporters with a TLR-9 Agonist Induces Neutralizing Antibodies and T Cell Memory. *ACS Cent Sci* **2021**, *7* (7), 1191-1204.
- 44. McKinlay, C. J.; Benner, N. L.; Haabeth, O. A.; Waymouth, R. M.; Wender, P. A. Enhanced mRNA delivery into lymphocytes enabled by lipid-varied libraries of charge-altering releasable transporters. *Proc Natl Acad Sci U S A* **2018**, *115* (26), E5859-E5866.

- 45. Testa, S.; Haabeth, O. A. W.; Blake, T. R.; Del Castillo, T. J.; Czerwinski, D. K.; Rajapaksa, R.; Wender, P. A.; Waymouth, R. M.; Levy, R. Fingolimod-Conjugated Charge-Altering Releasable Transporters Efficiently and Specifically Deliver mRNA to Lymphocytes In Vivo and In Vitro. *Biomacromolecules* **2022**, *23* (7), 2976-2988.
- 46. Adams, D.; Gonzalez-Duarte, A.; O'Riordan, W. D.; Yang, C. C.; Ueda, M.; Kristen, A. V.; Tournev, I.; Schmidt, H. H.; Coelho, T.; Berk, J. L., et al. Patisiran, an RNAi Therapeutic, for Hereditary Transthyretin Amyloidosis. *N Engl J Med* **2018**, *379* (1), 11-21.
- 47. Blake, T. R.; Waymouth, R. M. Organocatalytic ring-opening polymerization of morpholinones: new strategies to functionalized polyesters. *J Am Chem Soc* **2014**, *136* (26), 9252-5.
- 48. Olsen, P.; Odelius, K.; Albertsson, A. C. Thermodynamic Presynthetic Considerations for Ring-Opening Polymerization. *Biomacromolecules* **2016**, *17* (3), 699-709.
- 49. Hong, M.; Chen, E. Y. Completely recyclable biopolymers with linear and cyclic topologies via ring-opening polymerization of gamma-butyrolactone. *Nat Chem* **2016**, *8* (1), 42-9.
- 50. Yuan, R.; Xu, G.; Lv, C.; Zhou, L.; Yang, R.; Wang, Q. Bifunctional phosphazene-thiourea/urea catalyzed ring-opening polymerization of cyclic esters. *Materials Today Communications* **2020**, *22*, 100747.
- 51. Lin, B.; Waymouth, R. M. Urea Anions: Simple, Fast, and Selective Catalysts for Ring-Opening Polymerizations. *J Am Chem Soc* **2017**, *139* (4), 1645-1652.
- 52. Zhang, G.; Chen, J.; Payne, S. J.; Kooi, S. E.; Demas, J. N.; Fraser, C. L. Multi-Emissive Difluoroboron Dibenzoylmethane Polylactide Exhibiting Intense Fluorescence and Oxygen-Sensitive Room-Temperature Phosphorescence. *Journal of the American Chemical Society* **2007**, *129* (29), 8942-8943.
- 53. Meyer, R. A.; Neshat, S. Y.; Green, J. J.; Santos, J. L.; Tuesca, A. D. Targeting strategies for mRNA delivery. *Materials Today Advances* **2022**, *14*, 100240.
- 54. Decuzzi, P.; Godin, B.; Tanaka, T.; Lee, S. Y.; Chiappini, C.; Liu, X.; Ferrari, M. Size and shape effects in the biodistribution of intravascularly injected particles. *J Control Release* **2010**, *141* (3), 320-7.
- 55. Walkey, C. D.; Chan, W. C. Understanding and controlling the interaction of nanomaterials with proteins in a physiological environment. *Chem Soc Rev* **2012**, *41* (7), 2780-99.
- 56. Kaczmarek, J. C.; Kauffman, K. J.; Fenton, O. S.; Sadtler, K.; Patel, A. K.; Heartlein, M. W.; DeRosa, F.; Anderson, D. G. Optimization of a Degradable Polymer-Lipid Nanoparticle for Potent Systemic Delivery of mRNA to the Lung Endothelium and Immune Cells. *Nano Lett* **2018**, *18* (10), 6449-6454.
- 57. Yan, Y.; Xiong, H.; Zhang, X.; Cheng, Q.; Siegwart, D. J. Systemic mRNA Delivery to the Lungs by Functional Polyester-based Carriers. *Biomacromolecules* **2017**, *18* (12), 4307-4315.
- 58. Kaczmarek, J. C.; Patel, A. K.; Rhym, L. H.; Palmiero, U. C.; Bhat, B.; Heartlein, M. W.; DeRosa, F.; Anderson, D. G. Systemic delivery of mRNA and DNA to the lung using polymerlipid nanoparticles. *Biomaterials* **2021**, *275*, 120966.
- 59. Carrasco, M. J.; Alishetty, S.; Alameh, M. G.; Said, H.; Wright, L.; Paige, M.; Soliman, O.; Weissman, D.; Cleveland, T. E. t.; Grishaev, A., et al. Ionization and structural properties of mRNA lipid nanoparticles influence expression in intramuscular and intravascular administration. *Commun Biol* **2021**, *4* (1), 956.

- 60. Wei, T.; Cheng, Q.; Min, Y. L.; Olson, E. N.; Siegwart, D. J. Systemic nanoparticle delivery of CRISPR-Cas9 ribonucleoproteins for effective tissue specific genome editing. *Nat Commun* **2020**, *11* (1), 3232.
- 61. Dove, A. P.; Pratt, R. C.; Lohmeijer, B. G. G.; Waymouth, R. M.; Hedrick, J. L. Thiourea-Based Bifunctional Organocatalysis: Supramolecular Recognition for Living Polymerization. *Journal of the American Chemical Society* **2005**, *127* (40), 13798-13799.

Table of contents graphic:

